

Alma Mater Studiorum Università di Bologna
Archivio istituzionale della ricerca

The talar morphology of a hypochondroplastic dwarf: A case study from the Italian Late Antique period

This is the final peer-reviewed author's accepted manuscript (postprint) of the following publication:

Published Version:

Sorrentino, R., Carlson, K.J., Figus, C., Pietrobelli, A., Stephens, N.B., DeMars, L.J.D., et al. (2022). The talar morphology of a hypochondroplastic dwarf: A case study from the Italian Late Antique period. INTERNATIONAL JOURNAL OF OSTEOARCHAEOLOGY, 32, 429-443 [10.1002/oa.3078].

Availability:

This version is available at: <https://hdl.handle.net/11585/841830> since: 2022-06-28

Published:

DOI: <http://doi.org/10.1002/oa.3078>

Terms of use:

Some rights reserved. The terms and conditions for the reuse of this version of the manuscript are specified in the publishing policy. For all terms of use and more information see the publisher's website.

This item was downloaded from IRIS Università di Bologna (<https://cris.unibo.it/>).
When citing, please refer to the published version.

(Article begins on next page)

This is the final peer-reviewed accepted manuscript of: **Sorrentino R., Carlson K. J., Figus C., Pietrobelli A., Stephens N.B., DeMars L. J. D., Saers J. P. P., Armando J., Bettuzzi M., Guarnieri T., Oxilia G., Vazzana A., Parr W., Turley K., Morigi M.P., Stock J. T., Ryan T. M., Benazzi S., Marchi D., Belcastro M. G (2021). The talar morphology of a hypochondroplastic dwarf: A case study from the Italian Late Antique period. *International Journal of Osteoarchaeology*. The final published version is available online at: <https://doi.org/10.1002/oa.3078>**

Rights / License:

The terms and conditions for the reuse of this version of the manuscript are specified in the publishing policy. For all terms of use and more information see the publisher's website.

This item was downloaded from IRIS Università di Bologna (<https://cris.unibo.it/>)

When citing, please refer to the published version.

The talar morphology of a hypochondroplasic dwarf: A case study from the Italian Late Antique period.

Running head: In- and out the talus of an hypochondroplasic dwarf.

Rita Sorrentino^{1,2†}, Kristian J. Carlson^{3,4}, Carla Figus², Annalisa Pietrobelli¹, Nicholas B. Stephens⁵, Lily J. D. DeMars⁵, Jaap P.P. Saers⁶, Jessica Armando², Matteo Bettuzzi⁷, Tiziana Guarnieri^{1,8}, Gregorio Oxilia², Antonino Vazzana², William Parr⁹, Kevin Turley¹⁰, Maria Pia Morigi⁷, Jay T. Stock^{6,11,12}, Timothy M. Ryan⁵, Stefano Benazzi^{2,13*}, Damiano Marchi^{14,15*}, Maria Giovanna Belcastro^{1*}

†: Corresponding author

*: Equal contribution

¹Department of Biological, Geological and Environmental Sciences, University of Bologna, Bologna 40126, Italy.

²Department of Cultural Heritage, University of Bologna, Ravenna 48121, Italy.

³Department of Integrative Anatomical Sciences, Keck School of Medicine, University of Southern California, Los Angeles 90089, California.

⁴Evolutionary Studies Institute, University of the Witwatersrand, Palaeosciences Centre, Johannesburg, Wits 2050, South Africa.

⁵Department of Anthropology, The Pennsylvania State University, State College, PA 16802, USA
d Department of Biology, University of Pisa, Pisa 56126, Italy.

⁶Department of Archaeology, Cambridge University, Cambridge CB2 3EX, UK.

⁷Department of Physics and Astronomy, University of Bologna, Bologna 40127, Italy.

⁸Interuniversity Consortium "Istituto Nazionale Biostrutture e Biosistemi" (INBB-Biostructures and Biosystems National Institute), Rome 00136, Italy.

⁹Surgical and Orthopaedic Research Laboratories, Prince of Wales Hospital, University of New South Wales, Sydney 1466, Australia.

¹⁰Department of Anthropology, University of Oregon, Eugene, OR, 97403–1218, USA.

¹¹Department of Anthropology, Western University, London, Ontario N6A 3K7, Canada.

¹²Department of Archaeology, Max Planck Institute for the Science of Human History, Jena 07745, Germany.

¹³Department of Human Evolution, Max Planck Institute for Evolutionary Anthropology, Leipzig 04103, Germany.

¹⁴Department of Biology, University of Pisa, Pisa 56126, Italy.

¹⁵Centre for the Exploration of the Deep Human Journey, University of the Witwatersrand, Johannesburg, Wits 2050, South Africa.

Abstract

This project aims to test whether geometric morphometric (GM) and trabecular analyses may be useful tools in identifying talar characteristics related to hypochondroplasia.

We quantified the external and internal talar morphology of an hypochondroplastic dwarf (T17) from Modena (northern Italy) dated to the 6th century AD. External talar morphology of T17 was compared with a broad sample of modern human tali (n = 159) using GM methods. Additionally, a subsample of these tali (n = 41) was used to investigate whole talar trabecular changes in T17. Our results show that GM and trabecular analyses identify a combination of traits linked to the dwarfing disorder of hypochondroplasia. These traits include decreased scaled talar dimensions compared to normal-sized individuals, presence of an accessory antero-lateral talar facet, high bone volume fraction and high anisotropy values throughout the entire talus.

In our case study, hypochondroplasia does not appear to substantially modify external talar morphology probably due to the fast growth of the talus. We suggest that small talar dimensions are associated with hypochondroplasia. An antero-lateral talar facet may result from the talus and calcaneus coalition (i.e., talocalcaneal abnormal bridging) possibly related to an everted foot posture that was limited by overgrowth of the fibula. We suggest that high talar trabecular density and strut orientation provide insights into pathological development of the trabecular plates in T17. Finally, our study suggests that high talar trabecular density and strut orientation, and small talar dimensions, may be added as possible concomitant talar hallmarks for hypochondroplasia.

Keywords: skeletal dysplasia, geometric morphometrics; trabecular analysis; antero-lateral talar facet; functional morphology.

1. Introduction

In humans, the talus acts as a fulcrum in the ankle. It determines the ankle posture by linking the tibia and fibula superiorly (talocrural joint) to the calcaneus inferiorly (subtalar joint) and navicular distally (transverse joint). The morphology of the talus allows prediction of the potential range of plantar- and dorsi-flexion, inversion and eversion of the foot (Griffin et al., 2015; Huson, 1991). Furthermore, the talus supports body weight and maintains stability of the body with small lateral movements while standing and walking (Huson, 1991).

Recent studies have suggested that talar morphology varies in humans according to variation in levels of mobility, terrain characteristics, use of shoes and foot types (Moore et al., 2019; Peeters et al., 2013; Saers, Ryan, & Stock, 2018; Sorrentino et al., 2020a; Turley, White, & Frost, 2015), while sexual dimorphism does not influence talar morphology (Sorrentino et al., 2020b). Individuals with high levels of mobility, walking strictly barefoot or wearing minimalistic footwear along uneven terrain (e.g., hunter-gatherers) exhibit a talar shape that facilitates a broad range of talar motions, and also exhibit a talus that is characterized by high bone volume fraction, and thicker, less widely spaced trabeculae in respect to populations with a sedentary lifestyle and stiff shoes (Saers, Ryan, & Stock, 2018; Sorrentino et al., 2020a; Sorrentino et al., 2021; Turley, White, & Frost, 2015).

Talar variability is also partly a consequence of some pathological foot traits, such as planus or cavus foot. The talus of individuals clinically diagnosed with a flat-foot exhibits an orientation of the talo-navicular joint that is more horizontal than tali of a neutrally aligned foot, contributing to joint instability and likely medial arch collapse in the flat foot group (Peeters et al., 2013). Cavus-foot tali, in contrast, are characterized by extended lateral and medial tubercles, probably because of higher posterior loading (i.e., at the calcaneus) or for increased bony prominences in cavus feet (Moore et al., 2019).

More generally, foot deformities and malalignment may affect the normal weight-bearing axis of the lower limbs, ultimately modifying the offset of the knee to this hip-foot line (Desai et al., 2007; Lee et al., 2007). Despite the pivotal role of the talus in concurring in the alteration of the lower leg axis, to our knowledge no studies on skeletal remains have addressed how talar shape changes in individuals with altered gait mechanics, as in the case of dwarfism.

The present study focuses on the talus of an Italian Late Antique hypochondroplastic individual (Fig. 1; Traversari et al., 2020). Our aim is to analyze the talar shape of this individual using a large non-pathological (pre)historic and modern human dataset (Sorrentino et al., 2020a, 2021) as a reference in order to identify signals potentially related to the particular loading regime to which the talus is subjected in individuals affected by the dwarfism condition. In particular, we will combine Geometric Morphometric (GM) and trabecular analyses to assess external talar shape and internal

structure, respectively, and determine whether either approach may be a useful tool in diagnosing external and internal talar abnormalities related to hypochondroplasia. In our analysis we will also discuss the role of physiological and developmental factors characteristic of hypochondroplasia

2. Materials and Methods

In this study, we analyze the right talus of the hypochondroplastic young (~23–30 years of age at death) female individual (T17; Fig. 1) from Piazza XX Settembre burial site (Modena, northern Italy) dated to the 6th century AD and described by Traversari et al. (2020).

Achondroplasia is the most common form of disproportionate dwarfism in humans, with hypochondroplasia showing a similar but less severe condition than achondroplasia (Baujat et al., 2008; Horton, Hall, & Hecht, 2007; Wynne-Davies, Walsh, & Gormley, 1981).

The lower limbs of the T17 individual are characterized by bowing of the femora and tibiae (especially the left one) and coxa vara. The knee of T17 appears to exhibit a valgus posture (Fig. 2). Even if the *genu varum* is a clinical hallmark of achondroplasia, the valgus knee has been also identified in achondroplastic individuals (Sims et al., 2020).

The feet of T17 do not show remarkable anomalies or pathological modifications (Traversari et al., 2020). The T17 right talus is well preserved with small missing cortical and trabecular areas especially in the region of the talar head and neck (Fig. 3a), while the left talus is missing altogether. There are no external signs of pathological conditions such as osteophytes, bone anomalies, and fractures in the right talus. Inferiorly, along the posterior calcaneal facet, there is present an accessory antero-lateral talar facet (Fig. 3b).

The T17 right talus was scanned using a structured light three-dimensional (3D) surface scanner (Artec Space Spider, Artec 3D, Luxembourg) and the resulting 3D model was mirrored to be compared to a published left modern human tali comparative sample (Sorrentino et al., 2020a). The comparative sample consists of 160 tali from modern human groups representing the Middle Stone Age to the 20th century, and characterized by different mobility levels and include shod or unshod individuals. Sample composition is shown in Table 1 and consists of Upper Paleolithic individuals (Romito, Veneri and Villabruna; Giacobini, 2006) and Clark Howell Omo (Ethiopia) dated to Middle Stone Age (Parr et al., 2014); Black Earth hunter-gatherers (Carrier Mills Archaeological District, Illinois, USA) dated to the Late Archaic period (3000 B.C.; Jefferies, 2013); hunter-gatherers from San Francisco Bay (California; Turley, White, & Frost, 2015) belonging to the Shell Midden Cultures (~1500 B.C.–500 A.D.); mixed agricultural and hunting Norris Farms (Middle Woodland Oneota site of Norris Farms #36, Illinois, USA) dated to the Late Prehistoric North

America period (1300 A.D.; Santure et al., 1990); Paleo-Inuit individuals (Point Hope, Alaska) dated to ~1600–500 B.C. (Dumond, 2011); Egyptian farmers (~600–350 B.C.) from El Hesa (Francigny, de Voogt, Kahn, & Harcourt-Smith, 2014); Paleo Pueblo mountain dwellers from Canyon de Chelly (New Mexico) dated to ~1000 B.C. (Turley, White, & Frost, 2015); a mountain dweller group from Roccapelago (Italy, 17th–18th century; Traversari, 2017); Nguni individuals (Southern Africa, 20th century) from the Dart Collection housed at the University of Bologna; post-industrial revolution individuals of New York (United States) and Bologna (Italy) dated to 19th–20th century (Belcastro et al., 2017; Turley, White, & Frost, 2015). Individuals from Piazza Grande burial site in Modena (northern Italy, IV-VII century) were added to this sample as they are chronologically and geographically close to the Piazza XX Settembre burial site from which T17 was unearthed (Vazzana et al., 2017). The comparative samples include no apparent pathological tali of individuals for which sex was known (i.e., New York and Bologna) or anthropologically estimated.

A 3D template of 251 (semi)landmarks (15 landmarks, 105 curve semilandmarks and 131 surface semilandmarks) described in Sorrentino et al. (2020a, 2020b, 2020c) was applied to the target using Viewbox 4 software (dHAL software). Cartesian coordinates were superimposed (i.e., translated, scaled and rotated) using generalized Procrustes analysis (GPA) to compute shape coordinates, allowing the semilandmark coordinates to slide against recursive updates of the Procrustes consensus (Gunz, Mitteroecker, & Bookstein, 2005; Mitteroecker & Gunz, 2009; Slice, 2005) using the R package geomorph 3.3.2 (Adams, Collyer, Kaliontzopoulou, & Baken, 2021). Shape coordinates of the comparative sample only were used to perform a Principal Component Analysis (PCA) where the predicted principal component (PCs) scores of the T17 talus were projected into this space to evaluate its morphological variation in relation to the modern human groups (Sorrentino et al., 2020b, 2020c). A permutation test ($n = 10000$) using the first 3 principal components (PCs), which account for collectively 28.6% of variance (Bailey et al., 2020), was conducted to identify shape differences among modern human groups using the R package Morpho v. 2.8 (Schlager, 2017). The analyses were performed in R v. 4.0.3 (R Core Team, 2020). Shape changes along principal axes were obtained by thin-plate spline (TPS) deformation of the Procrustes mean shape surface (Bookstein, 1991) in Avizo 9.2 (Thermo Fisher Scientific, Waltham).

Talar size was evaluated as the square root of the summed squared distances between each (semi)landmark and the centroid of the (semi)landmark configuration (i.e., centroid size) and visualized using box plots. A form space PCA (i.e., shape + size) was computed by adding the natural logarithm of centroid size to the Procrustes shape coordinates (Klingenberg, 2016) to evaluate size-shape variation of T17 with respect to the comparative sample. While sexual dimorphism might not influence talar morphology, it can influence talar size (Sorrentino et al.,

2020b). Therefore, talar size of the female T17 individual was compared with the overall sample (males, females and individual with sex unknown) and a subsample of females only (N = 63).

A subsample of individuals characterized by different levels of mobility and subsistence strategies was selected for comparison to T17 using whole bone trabecular analysis (Black Earth hunter-gatherers, agriculturalist Norris Farms and post-industrial revolution individuals of Bologna; Table 1). We arbitrarily selected highly mobile hunter-gatherers, intermediate in mobility agriculturalist and sedentary post-industrial individuals to represent different levels of mobility and varied subsistence strategies since these are suggested to be associated with differences in human foot trabecular structure (DeMars et al., 2021; Saers, Ryan, & Stock, 2018; Sorrentino et al., 2021).

Scans for Norris Farms, Black Earth, and Bologna tali were obtained by using the industrial microCT (OMNI-X HD600 High-Resolution X-ray computed tomography - HRCT) at the Center for Quantitative Imaging (CQI) at the Pennsylvania State University using source energy settings of 180 kV, 110 mA, and between 2800 and 4800 views (0.030-0.057 mm). MicroCT scans for the T17 talus used a voxel resolution of 0.040 mm (78 kV, 200 μ A) and were obtained at the Department of Physics and Astronomy, University of Bologna (Bologna, Italy) with an in-house CT system (Kevex PXS10-65 microfocus X-ray tube and Varian PaxScan 2520D flat-panel X-ray detector; Albertin, Bettuzzi, Brancaccio, Morigi, & Casali, 2019).

Image sequences from microCT data were down-sampled to 8-bit in ImageJ v. 1.52a (NIH, Bethesda, Maryland, USA). Segmentation of volumes was performed using the MIA-Clustering algorithm (Dunmore, Wollny, & Skinner, 2018), while quantification and visualization of bone volume fraction (BV/TV), degree of anisotropy (DA), trabecular thickness (Tb.Th), trabecular number (Tb.N), and trabecular spacing (Tb.S) were performed using Medtool v4.2 (Dr. Pahr Ingenieure e.U, 2018) (Gross, Kivell, Skinner, Nguyen, & Pahr, 2014). Herein a series of masks were used to remove the cortical mask from the 3D mask, which allows for quantification of trabecular bone volume (BV) to total volume (TV) and relative orientation (DA) via a series of 7.5 mm volumes of interest (VOI) at each node of a 3.5 mm grid overlaid onto the 3D volume.

Hereafter, we followed the Phenotypic PointCloud Analysis protocol described in DeMars et al. (2021) to map site-specific BV/TV and DA group average values. Briefly, a set of pseudolandmarks was automatically positioned on the trabecular volume of each individual using a modified version of the 'auto3dgm' in the 'geomorph' v. 3.3.1 R package (Boyer et al., 2015; Tingran et al., 2020) and a GPA was performed to find the mean shape coordinates representing the sample average. Then, we warped the closest-to-the-mean specimen to the mean shape coordinates obtained from the GPA (Stephens et al., 2018). The average mesh obtained was then tetrahedralized employing evenly-spaced points using TetWild (Hu et al., 2018) and the vertices of the tetrahedral mesh were finally converted to a point cloud. Point clouds were then obtained for each individual through the

interpolation of BV/TV and DA scalar values to the vertices of the tetrahedral mesh. Then, they were aligned by applying the auto3dgm transformation matrices and then registered with a rigid, affine, and deformable alignment using a python implementation of the Coherent Point Drift algorithm (Myronenko & Song, 2010). Whereas mapping of BV/TV and DA for T17 was performed by interpolating results from the VOIs onto its tetrahedral mesh of trabecular volume (Gross et al., 2014).

Mean trabecular thickness (Tb.Th, mm) and spacing (Tb.Sp, mm) were calculated from the average diameter of seeded spheres grown within the trabecular or internal space, respectively (Hildebrand & Rüegsegger, 1997). Tb.N is based on both thickness and spacing using the formula $1/(Tb.Th + Tb.Sp)$. A Kruskal–Wallis test with intergroup pairwise comparison (i.e., Dunn test with a Bonferroni correction) was performed for each mean talar trabecular parameter, with the distribution and mean trabecular parameters across the sample visualized via violin plots.

Considering that adult trabecular bone might be influenced by age-related bone loss (Lochmüller et al., 2008), and that T17 has an age-at-death estimated between 23–30 years, variation of trabecular parameters for Norris Farms (mean age 28.4 ± 7.2), Black Earth (mean age 36.4 ± 9.4), and Bologna (mean age 44.7 ± 24.1) in relation to age was assessed using two-tailed t-tests for the pooled-age samples subdivided into individuals younger and older than 35 years old.

3. Results

3.1 Talar size

Talar size (i.e., centroid size) of T17 is smaller than those of the overall comparative groups and female only groups (Fig. 4, Table 2). Specifically, centroid size of the T17 talus is below the lower quartiles of each group, including the chronologically and geographically close Modena group. However, some individuals from Egyptian, Point Hope and Black Earth groups present small tali approaching that of T17 as shown by the extremes of their ranges (Fig. 4a), although T17 is at least one standard deviation (SD) below each group average (Table 2). Individuals of the comparative groups most closely resembling T17 are mainly females (Fig. 4b). Talar size of T17 is three SDs below the Modena group average and the Modena female average, and four SDs below the Modena male average (Table 2). Considering the form space PCA plot, T17 is positioned on the extreme negative side of PC1 along with a few small tali of the comparative sample (Fig. 4c), which are mainly female individuals (Fig. 4d). While grouping along PC1 is related to size variation, PC2 separates groups according to mobility characterization, with more mobile groups occupying the positive region and more sedentary groups the negative region. T17 plots in the middle of the PC2 axis near zero.

3.2 External talar shape

The shape space PCA plot (Fig. 5) and permutation tests using the first three PCs (Table 3) show that talar shape tends to separate more mobile (i.e., Upper Paleolithic/Middle Stone Age group, Californian, Black Earth and Norris Farms) and more sedentary groups (i.e., Bologna and New York), as previously observed by Sorrentino et al. (2020a).

The Modena group occupies the central part of the PCA plot along with groups characterized by intermediate mobility (Fig. 5). In PC1 (14.4 %) vs. PC2 (8.3 %), T17 falls in the range of variation of the Modena group (Fig. 5a). However, T17 diverges from the Modena group along PC3 (5.7 %), falling more on the positive side of PC3 (Fig. 5b).

Primary differences in talar morphology across the sample are detected along PC1 (14.4 %), where extreme positive scores (hunter-gatherers) reflect the presence of a wider talar neck and head, a relatively shortened neck, increased dorsal convexity of the trochlea, a mediolaterally wider anterior margin of the trochlea with an anterior extension of the medial margin, lateral displacement of the lateral malleolar facet, increased medial malleolar facet cupping, and a more concave posterior calcaneal facet when compared to extreme negative PC1 scores exhibited by sedentary groups (Fig. 5). The talus of T17 (Fig. 3) shows a mix of features that are in part shared with hunter-gatherers (e.g., a short and broad neck, a mediolaterally enlarged head, a dorsally more convex trochlea, and an anteriorly extended medial trochlear margin), post-industrial groups (e.g., similar widths of anterior and posterior margins of the trochlea and a less cupped medial malleolar facet), and intermediate in mobility groups (e.g., modestly lateral projection of the lateral malleolar facet and modestly concavity of the posterior calcaneal facet).

Along PC2 (8.3%) and PC3 (5.7%), talar shape differences are less marked than those expressed by the extreme PC1 scores. The talus of T17 plots exactly in the middle of the PC2 axis, where positive PC2 scores reflect a posterior extension of the medial margin of the navicular facet, a broad anterior-medial calcaneal facet, and a more oval and concave posterior calcaneal facet when compared with negative PC2 scores. Whereas, along PC3, T17 falls more toward positive scores, which are characterized by less inferiorly and posteriorly projecting medial and lateral tubercles, a mediolaterally elongated and less concave posterior calcaneal facet, a slightly more dorsally convex trochlea and a more antero-posteriorly extended medial malleolar facet compared to negative PC3 scores (Fig. 5).

3.3 Internal talar structure

Violin plots of trabecular parameters for each population and T17 are illustrated in Figure 6.

Mean and standard deviation of BV/TV, DA, Tb.N, Tb.Sp and Tb.Th are summarized in Table 4. No significant differences were found between groups of individuals younger and older than 35 years for each trabecular parameter. Whereas, significant differences in the overall talar mean trabecular parameters among populations are detected in BV/TV, DA, Tb.SP and Tb.Th, but are not detected in Tb.N (Fig. 6 and Table 5).

The highly mobile Black Earth individuals are characterized by high talar trabecular density, and thick and less spaced trabeculae (Fig. 6 and Table 4). On the contrary, the less mobile Norris Farms and Bologna groups exhibit lower BV/TV and more widely spaced trabeculae with respect to Black Earth, but trabecular thickness significantly differs only between Black Earth and Norris Farms (Fig. 6 and Tables 4-5). Norris Farms individuals are significantly different in DA from Black Earth and Bologna individuals (Table 5). T17 shows the highest mean value of BV/TV similar to Black Earth individuals, but for the high mean value of DA and lower mean value of Tb.Th T17 is more similar to Norris Farms (Table 4).

Besides the mean talar trabecular properties, BV/TV and DA distributions throughout the talus show that T17 has higher peaks of both BV/TV and DA when compared to the talar average of each group (Fig. 7). In particular, although T17 is more similar to Black Earth in global values of the talus, it shows higher trabecular density along with the head and neck dorso-lateral and dorso-medial region, lateral aspect of the posterior calcaneal facet, lateral malleolar facet and medial aspect of the talar corpus. Furthermore, T17 shows lower BV/TV in the region of the trochlea when compared to Black Earth, and it resembles the trochlear region of both Bologna and Norris Farms in local magnitude. Similarly, T17 presents higher DA values throughout the entire talar trabecular structure with respect to the talar average of each group. It appears more anisotropic in the talar head, neck and superolateral aspect of the talus, which is a pattern observed also in the comparatively lower DA Black Earth individuals (Fig. 7).

4. Discussion

4.1 Talar size

The talus of the hypochondroplastic young female individual (T17) from a 6th century AD Modena burial site (northern Italy) exhibits reduced dimension and falls at least one SD below means of modern human comparative groups, even when considering a female only sample (Fig. 4, Table 2). Particularly, the talar size of T17 is three SDs below the chronologically and geographically close Modena group (Table 2; also compare the T17 talus with a talus of a Modena individual illustrated in Fig. 3).

The feet of individuals affected by achondroplasia and hypochondroplasia are described as “normal”, or sometimes as broader and longer in relation to shorter legs (Sims et al., 2019; Sims et

al., 2020; Slon et al., 2013; Traversari et al., 2020; Waters-Rist & Hoogland, 2013). These genetic conditions affect endochondral bone formation, and bones characterized by the least number of growth plates (e.g., the femur and humerus both have only two growth plates) tend to be shortened. Then, the foot bones, which have a cumulatively higher number of growth plates (considering toes and tarsals together), are less severely shortened, appearing proportionately longer relative to the other lower limb bones when compared to individuals without the dwarfing disorder (Ortner, 2003; Sims et al., 2019, 2020). However, considering each bone in isolation, the absolute sizes of individual bones affected by endochondral ossification (including those of the foot) are still shortened compared to those of unaffected individuals (Ortner, 2003; Slon et al., 2013). This is confirmed by our analyses showing a remarkably small (in all dimensions) talus in the hypochondroplastic individual T17 (Fig. 4, Table 2).

4.2 External talar shape

The T17 talus is characterized by a short and broad neck, a mediolaterally enlarged head, a dorsally more convex trochlea, and an anteriorly extended medial trochlear margin (Figs. 3 and 5). A short and wide talar neck suggests increased loading of the medial column of the foot during push-off, which is generally interpreted as a result of walking and carrying out habitual activities without wearing rigid foot coverings in more mobile groups (Jashashvili et al., 2015; Sorrentino et al., 2020a; Trinkaus, 2005). Similarly, individual T17 has likely exercised great loading at push-off, similar to barefoot hunter-gatherers or those wearing minimalistic soft-coverings, though such an explanation is highly improbable as the sole explanation for our finding given the low mobility of hypochondroplastic individuals (Haga, 2004; Sims et al., 2020, 2019). Indeed, recent kinematic studies on the gait cycle have shown that individuals with achondroplasia walk at a slower speed, have shorter stride lengths and higher frequencies of strides compared with a group of healthy individuals, largely because of the shorter, disproportionate leg length of the former (Sims et al., 2019, 2020). High stride frequencies in T17 may be a contributing factor to the more robust (i.e., short and broad) talar neck likely due to higher load given more impacts per given distance, though kinematic studies on hypochondroplastic individuals would be necessary to test this hypothesis.

The talus of T17 shows a dorsally more convex trochlea similar to the hunter-gatherer groups in our sample. This feature is supposed to reflect a broader range of ankle dorsal and plantar flexion necessary to traverse uneven terrain while wearing minimalistic soft-coverings and/or habitual passive dorsiflexion such as occurs during squatting (Carlson, Grine, & Pearson, 2007; Sorrentino et al., 2020a). Therefore, increased ankle dorsiflexion in T17 could be interpreted as a consequence of the hypochondroplastic condition. Accordingly, Sims and colleagues (2019, 2020) have observed that achondroplastic individuals exhibit more flexed knee and ankle joints over the entire gait cycle,

likely due to a higher foot/leg length ratio. More flexed lower limb joints (e.g., hip, knee, and ankle) may help to avoid toe contact with the ground during swing phase and thus maintain gait proficiency (Sims et al., 2019, 2020).

Other characteristics observed in T17 external talar morphology are an equally wide anterior and posterior margin of the trochlea, and a less cupped medial malleolar facet, which are also observed in post-industrial groups. T17 also shows a lateral projection of the lateral malleolar facet and a concavity of the posterior calcaneal facet that fall within the range of intermediate mobility in the comparative groups (Figs. 3 and 5). A less cupped medial malleolar facet and a modestly projecting lateral malleolar facet of the talus likely reflect a neutral foot posture in the T17 individual (Sorrentino et al., 2020a). However, lateral displacement of the lateral malleolar facet and increased medial malleolar facet cupping (observed also in hunter-gatherers) may reflect a more everted foot in T17 while standing and walking (Sorrentino et al., 2020a; Sparacello, Marchi, & Shawn 2014). Finally, a less concave posterior calcaneal facet in T17 suggests a limited range of inversion and eversion at the subtalar joint (Sorrentino et al., 2020a), in contrast with the observed valgus knee of T17 (Fig. 2), which has been described to elicit a more everted hindfoot (Sims et al., 2020).

Further understanding of the external and internal morphology of the T17 talus may be gained by considering developmental modification of a hypochondroplastic individual. Before reaching skeletal maturity, the faster rate of growth of the fibula with respect to the tibia and laxity in lateral collateral ligaments in achondroplastic individuals may lead to limited eversion of the hindfoot, contributing to the formation of an inverted foot and varus knee (Lee et al., 2007). In achondroplastic individuals the knee is usually in a varus position that, together with tibial bowing, may cause limitations in knee and ankle joint motions, waddling gait, and/or knee instability (Ain et al., 2006; Hunter et al., 1998; Pauli, 2019). However, in T17 both knees are in a valgus position (Fig. 2), which is a posture that may be present in achondroplastic individuals (Sims et al., 2020). Therefore, relatively faster growth of the fibula and laxity in lateral collateral ligaments preceding skeletal maturity in the hypochondroplastic T17 may have limited eversion of the hindfoot in this individual, despite the presence of a valgus knee in T17 which would have elicited a more everted hindfoot (Lee et al., 2007; Ortner, 2003). Limited inversion and eversion at the subtalar joint may also correlate with the presence of the accessory antero-lateral talar facet in T17, suggesting talocalcaneal abnormal bridging, i.e. tarsal coalition (Vossen et al., 2020) or atypical structure of the subtalar joint. In addition, the accessory antero-lateral talar facet may have altered foot mechanics, causing pain at the lateral side of the hindfoot and inflamed soft tissues such as talocalcaneal ligaments (Hattori et al., 2015; Kurashige, 2017; Niki et al., 2014).

4.3 Internal trabecular structure

T17 exhibits more widespread high density and alignment regions throughout the talus than the comparative groups (Fig. 7), also when considering as separate groups individuals younger and older than 35 years (Table 4). Particularly, T17 is most similar to the highly mobile Black Earth individuals for the high values of BV/TV (Figs. 6-7 and Table 4). It is unlikely though that the explanation of these features is due to high levels of physical activity for T17, as it could be argued for Black Earth individuals. T17 also increased stereotyped (i.e., more selectively oriented) loading at the medial side of the foot (Fig. 7), probably a consequence of altered locomotion due to the skeletal dysplasia experienced by this individual. Indeed, considering that achondroplasia is a genetic condition that negatively affects locomotor performance (Haga, 2004; Sims et al., 2020, 2019), increased medial loading localized on the talar head and neck may relate to a greater degree of foot supination retained during development, which has been similarly reported in achondroplastic individuals (Kiernan, 2021). High BV/TV and DA values along the lateral side of the T17 talus (Fig. 7) suggest high levels of loading on the lateral side of the foot. This would be consistent with passive eversion during stance phase. While limited eversion of the hindfoot of T17 is suggested by the shape of the less concave posterior calcaneal facet, the high BV/TV and DA values along the lateral side suggest that this individual may have been experiencing passive hindfoot eversion, inducing an abnormal subtalar osseous contact in the lateral side of the *sinus tarsi*, which would also explain the etiology of an accessory antero-lateral talar facet (Fig. 3) (Alqahtani et al., 2020; Hattori et al., 2015; Kurashige, 2017). The valgus knee condition, which is present in T17 (Fig. 2), may also be a contributing factor to suggested lateral loading of the foot, given the laxity of ankle collateral ligaments observed in such a condition (Pauli, 2019).

Trabecular parameters are likely to reflect altered development of the trabecular plates (Colombo et al., 2018). Our results highlight higher BV/TV and DA throughout the whole talus of T17, corroborating the findings of Colombo and colleagues (2018) who showed that trabecular organizational changes in genetic dwarfism from the perinatal period revealed higher density and greater strut alignment. This is due to endochondral histogenesis of the plates that are characterized by wider *septa* (i.e., future trabeculae) being retained for a longer time with respect to those of individuals without the dwarfing disorder, leading to a more vertically oriented and thickened trabecular mesh (Colombo et al., 2018). Less spaced and thick trabeculae of individuals in the Black Earth group (Fig. 6 and Table 4) are associated with high values of BV/TV. Similarly, results reported in Saers et al. (2018) show thick trabeculae in the talus of the highly mobile Black Earth group, which are also associated with high values of BV/TV, but this coupling is not reflected in T17, which possess more intermediate values of Tb.Th (Fig. 6 and Table 4).

5. Conclusion

Our results suggest that hypochondroplasia of the T17 individual, despite inducing peculiar morphological features, does not severely modify its external talar morphology. This is probably due to rapid growth of the talus, which may have achieved an adult configuration at 8-11 years (Scheuer & Black, 2004), relatively early with respect to leg bones where a slower cartilage-to-bone turnover caused bowing of the femora and tibia (Traversari et al., 2020). Overall, the fast talar development guarantees conservative talar external morphology even in the presence of hypochondroplasia, while the main changes distinguishing T17 are observed as reduced talar size and comparatively higher bone volume fraction and anisotropy.

High levels of ankle dorsiflexion and the presence of an antero-lateral talar facet may be associated with the hypochondroplastic condition of T17. Greater ankle dorsiflexion may compensate for an increased foot/leg length ratio by preventing toe contact with the ground during swing phase of the gait cycle (Sims et al., 2019, 2020). The observed antero-lateral talar facet in T17 may result from the talus and calcaneus coalition (i.e., talocalcaneal abnormal bridging) due to the tendency towards an everted foot posture that is limited by overgrowth of the fibula, ultimately resulting in high and oriented loading along the lateral side of the talus (Alqahtani et al., 2020; Hattori et al., 2015; Lee et al., 2007).

This study exemplifies how the combination of GM and trabecular approaches facilitates identification of two possible concomitant factors as talar hallmarks for hypochondroplasia: a conservative talar external morphology but with reduced size, and high BV/TV and DA. We suggest the use of both approaches when studying the talus, and even other bones, to obtain a more comprehensive set of results, and these two sets of results can be used to help inform one another. For example, the small size alone of an isolated talus may simply indicate a small individual without the dwarfing disorder. Similarly, high BV/TV and DA on an isolated talus may indicate both a hypochondroplastic individual or a highly mobile individual without the dwarfing disorder. Given that both loading patterns and the unique genetic condition of T17 may contribute to the form of the hypochondroplastic talus, we encourage the use of both GM and trabecular analyses when studying isolated tali.

The limitations of this study include the fact that it focused only on a single talus of an hypochondroplastic individual. These are in fact rare in the archaeological record. It is possible that by increasing the sample size of hypochondroplastic individuals we could confirm the effect of this dwarfing condition on the morphology of the talus. Further, increasing the size of the comparative sample may better elucidate the way in which other factors (e.g., sex, age, genetic background) may interact with internal and external talar shape variation. Though further studies are needed to test our hypotheses of the representativeness of the dwarfing condition, this first case study provides the

initial knowledge of talar plasticity related to hypochondroplastic dwarfism.

Acknowledgements

We are grateful to the curators and collections managers Natasha Johnson and Paolo Pellegatti of the P.A. Hearst Museum, UC Berkeley, for access to the Native American collection; Norman Macleod for access to the NHM's Konica Minolta scanner; T. Stecko and W. Yetter at the Penn State Center for Quantitative Imaging; Silvia Pellegrini (Municipal Museum of Archaeology and Ethnology of Modena) and Cinzia Cavallari (Soprintendenza Archeologica, Belle Arti e Paesaggio per le provincie di Bologna, Modena, Reggio Emilia e Ferrara) for access to T17 and the Modena sample; the curators of the Museo Delle Mummie di Roccapelago for access to the Roccapelago sample and Mirko Traversari for anthropological and historical information provided for this population. We thank Francesco Feletti, Luisa Mingozi and Denis Nicolini of the Unit of Radiology (S. Maria delle Croci Hospital of Ravenna) for providing scans for Italian collections.

Funding: This work was supported by the European Research Council (ERC) under the European Union's Horizon 2020 research and innovation program (grant number 724046, SUCCESS; www.erc-success.eu) awarded to SB, the National Science Foundation (grant/award number BCS-1847806) to TMR and LJDD, and the National Science Foundation Graduate Research Fellowship Program (grant number DGE1255832) to LJDD. Any opinions, findings, and conclusions or recommendations expressed in this material are those of the authors and do not necessarily reflect the views of the National Science Foundation.

Conflict of interest

The authors declare no potential conflict of interest.

Data Availability Statement

The data that support the findings of this study are available from the corresponding author upon reasonable request.

References

- Adams, D., Collyer, M. L., Kaliontzopoulou, A., & Baken, E. (2021). Geomorph: Software for geometric morphometric analyses. R package version 3.3.2. <https://cran.r-project.org/package=geomorph>.
- Ain, M. C., Shirley, E. D., Pirouzmanesh, A., Skolasky, R. L., & Leet, A. I. (2006). Genu varum in achondroplasia. *Journal of Pediatric Orthopaedics*, 26(3), 375–379. <https://doi.org/10.1097/01.bpo.0000203013.04272.b6>
- Albertin, F., Bettuzzi, M., Brancaccio, R., Morigi, M. P., & Casali, F. (2019). X-Ray computed tomography in situ: An opportunity for museums and restoration laboratories. *Heritage*, 2(3), 2028–2038. <https://doi.org/10.3390/heritage2030122>
- Alqahtani, E., Fliszar, E., Resnick, D. L., & Huang, B. K. (2020). Accessory anterolateral talar facet associated with tarsal coalition: prevalence and cross-sectional characterization. *Skeletal Radiology*, 49(3), 417–424. <https://doi.org/10.1007/s00256-019-03293-y>
- Bailey, S. E., Sorrentino, R., Mancuso, G., Hublin, J. J., & Benazzi, S. (2020). Taxonomic differences in deciduous lower first molar crown outlines of *Homo sapiens* and *Homo neanderthalensis*. *Journal of Human Evolution*, 147, 102864. <https://doi.org/10.1016/j.jhevol.2020.102864>
- Baujat, G., Legeai-Mallet, L., Finidori, G., Cormier-Daire, V., & Le Merrer, M. (2008). Achondroplasia. *Best Practice and Research: Clinical Rheumatology*, 22(1), 3–18. <https://doi.org/10.1016/j.berh.2007.12.008>
- Belcastro, M.G., Bonfiglioli, B., Pedrosi, M.E., Zuppello, M., Tanganelli, V., Mariotti, V. (2017). The history and composition of the identified human skeletal collection of the Certosa cemetery (Bologna, Italy, 19th–20th century). *International Journal of Osteoarchaeology*, 27, 912–925.
- Bookstein, F. L. (1991). *Morphometric tools for landmark data: geometry and biology*. Cambridge University Press.
- Boyer, D.M., Puente, J., Gladman, J.T., Glynn, C., Mukherjee, S., Yapuncich, G.S., Daubechies, I. (2015). A new fully automated approach for aligning and comparing shapes. *The Anatomical Record*, 298, 249–276.
- Carlson, K. J., Grine, F. E., & Pearson, O. M. (2007). Robusticity and sexual dimorphism in the postcranium of modern hunter-gatherers from Australia. *American Journal of Physical Anthropology*, 134(1), 9–23. <https://doi.org/10.1002/ajpa.20617>
- Colombo, A., Hoogland, M., Coqueugniot, H., Dutour, O., & Waters-Rist, A. (2018). Trabecular bone microarchitecture analysis, a way for an early detection of genetic dwarfism? Case study of a dwarf mother's offspring. *International Journal of Paleopathology*, 20, 65–71. <https://doi.org/10.1016/j.ijpp.2017.12.002>
- DeMars, L. J. D., Stephens, N. B., Saers, J. P. P., Gordon, A., Stock, J. T., & Ryan, T. M. (2021). Using point clouds to investigate the relationship between trabecular bone phenotype and behavior: An example utilizing the human calcaneus. *American Journal of Human Biology*, 33(2), e23468. <https://doi.org/10.1002/ajhb.23468>
- Desai, S. S., Shetty, G. M., Song, H. R., Lee, S. H., Kim, T. Y., & Hur, C. Y. (2007). Effect of foot deformity on conventional mechanical axis deviation and ground mechanical axis deviation during single leg stance and two leg stance in genu varum. *Knee*, 14(6), 452–457. <https://doi.org/10.1016/j.knee.2007.07.009>
- Dumond, D. E. (2011). *Archaeology on the Alaska Peninsula: The Northern Section: Fifty Years Onward*. Eugene, OR: University of Oregon Anthropological Papers 70.
- Dunmore, C. J., Wollny, G., & Skinner, M. M. (2018). MIA-Clustering: a novel method for segmentation of paleontological material. *PeerJ*, 6, e4374. <https://doi.org/10.7717/peerj.4374>
- Francigny, V., de Voogt, A., Kahn, J., & Harcourt-Smith, W. E. H. (2014). At the border between Egypt and Nubia: Skeletal material from El Hesa cemetery 2. *Journal of Ancient Egypt Interconnections*, 6, 5–10.

- Giacobini, G. (2006). Les sépultures du Paléolithique supérieur: la documentation italienne. *Comptes Rendus Palevol*, 5, 169-176.
- Griffin, N. L., Miller, C. E., Schmitt, D., & Ao, K. D. (2015). Understanding the evolution of the windlass mechanism of the human foot from comparative anatomy: Insights, obstacles, and future directions. *American Journal of Physical Anthropology*, 156, 1–10. <https://doi.org/10.1002/ajpa.22636>
- Gross, T., Kivell, T. L., Skinner, M. M., Nguyen, N. H., & Pahr, D. H. (2014). A CT-image-based framework for the holistic analysis of cortical and trabecular bone morphology. *Palaeontologia Electronica*, 17(3), 1–13.
- Gunz, P., Mitteroecker, P., & Bookstein, F. L. (2005). Semilandmarks in three dimensions. In Slice, D. E. (Ed.), *Modern morphometrics in physical anthropology* (pp. 73–98). New York, Springer.
- Haga, N. (2004). Management of disabilities associated with achondroplasia. *Journal of Orthopaedic Science*, 9(1), 103–107. <https://doi.org/10.1007/s00776-003-0729-4>
- Hattori, K., Sakuma, E., Nakayama, M., Kozaki, A., Wada, I., & Otsuka, T. (2015). An anatomic study of the accessory anterolateral talar facet. *Folia Morphologica (Poland)*, 74(1), 61–64. <https://doi.org/10.5603/FM.2015.0010>
- Hildebrand, T., & Rüegsegger, P. (1997). A new method for the model-independent assessment of thickness in three-dimensional images. *Journal of Microscopy*, 185(1), 67–75. <https://doi.org/10.1046/j.1365-2818.1997.1340694.x>
- Horton, W. A., Hall, J. G., & Hecht, J. T. (2007). Achondroplasia. *Lancet*, 370(9582), 162–172. [https://doi.org/10.1016/S0140-6736\(07\)61090-3](https://doi.org/10.1016/S0140-6736(07)61090-3)
- Hu, Y., Zhou, Q., Gao, X., Jacobson, A., Zorin, D., & Panozzo, D. (2018). Tetrahedral meshing in the wild. *ACM Trans. Graph.*, 37(4), 60-1.
- Hunter, A. G. W., Bankier, A., Rogers, J. G., Sillence, D., & Scott, C. I. (1998). Medical complications of achondroplasia: A multicentre patient review. *Journal of Medical Genetics*, 35(9), 705–712. <https://doi.org/10.1136/jmg.35.9.705>
- Huson, A. (1991). Functional anatomy of the foot. *Disorders of the Foot and Ankle*, 1, 409–431.
- Jashashvili, T., Dowdeswell, M. R., Lebrun, R., & Carlson, K. J. (2015). Cortical structure of hallucal metatarsals and locomotor adaptations in hominoids. *PloS one*, 10(1), e0117905. <https://doi.org/10.1371/journal.pone.0117905>
- Jefferies, R. W. (2013). *The Archaeology of Carrier Mills: 10,000 Years In The Saline Valley of Illinois*. Southern Illinois University Press, Carbondale.
- Kiernan, D. (2021). Lower limb biomechanics during gait in children with Achondroplasia. *Journal of Biomechanics*, 119, 110313.
- Klingenberg, C. P. (2016). Size, shape, and form: concepts of allometry in geometric morphometrics. *Development Genes and Evolution*, 226(3), 113–137. <https://doi.org/10.1007/s00427-016-0539-2>
- Kurashige, T. (2017). Accessory anterolateral talar facet impingement with tibialis spastic varus foot. *SAGE Open Medical Case Reports*, 5, 2050313X1774521. <https://doi.org/10.1177/2050313x17745210>
- Lee, S. T., Song, H. R., Mahajan, R., Makwana, V., Suh, S. W., & Lee, S. H. (2007). Development of genu varum in achondroplasia. *Journal of Bone and Joint Surgery - Series B*, 89(1), 57–61. <https://doi.org/10.1302/0301-620X.89B1.18223>
- Lochmüller, E.-M., Matsuura, M., Bauer, J., Hitzl, W., Link, T. M., Müller, R., & Eckstein, F. (2008). Site-specific deterioration of trabecular bone architecture in men and women with advancing age. *Journal of Bone and Mineral Research*, 23, 1964–1973.
- Mitteroecker, P., & Gunz, P. (2009). Advances in Geometric morphometrics. *Evolutionary Biology*, 36(2), 235–247. <https://doi.org/10.1007/s11692-009-9055-x>
- Moore, E. S., Kindig, M. W., McKearney, D. A., Telfer, S., Sangeorzan, B. J., & Ledoux, W. R. (2019). Hind- and midfoot bone morphology varies with foot type and sex. *Journal of Orthopaedic Research*, 37(3), 744–759. <https://doi.org/10.1002/jor.24197>
- Myronenko, A., & Song, X. (2010). Point set registration: Coherent point drift. *IEEE transactions*

on pattern analysis and machine intelligence, 32(12), 2262-2275.

- Niki, H., Hirano, T., Akiyama, Y., & Beppu, M. (2014). Accessory talar facet impingement in pathologic conditions of the peritalar region in adults. *Foot and Ankle International*, 35(10), 1006–1014. <https://doi.org/10.1177/1071100714540891>
- Ortner, D. J. (2003). *Identification of pathological conditions in human skeletal remains*. Academic Press.
- Parr, W.C.H., Soligo, C., Smaers, J., Chatterjee, H.J., Ruto, A., Cornish, L., Wroe, S. (2014). Three - dimensional shape variation of talar surface morphology in hominoid primates. *Journal of Anatomy*, 225(1), 42 – 59.
- Pauli, R. M. (2019). Achondroplasia: A comprehensive clinical review. In *Orphanet Journal of Rare Diseases*, 14(1), 1-49. <https://doi.org/10.1186/s13023-018-0972-6>
- Peeters, K., Schreuer, J., Burg, F., Behets, C., Van Bouwel, S., Dereymaeker, G., Sloten, J.V., & Jonkers, I. (2013). Altered talar and navicular bone morphology is associated with pes planus deformity: A CT-scan study. *Journal of Orthopaedic Research*, 31(2), 282–287. <https://doi.org/10.1002/jor.22225>
- R Core Team (2020). R: A language and environment for statistical computing. R Foundation for Statistical Computing, Vienna, Austria. <https://www.R-project.org/>.
- Saers, J.P.P., Ryan, T. M., & Stock, J. T. (2018). Trabecular bone functional adaptation and sexual dimorphism in the human foot. *American Journal of Physical Anthropology*, 168(1), 154-169. <https://doi.org/DOI: 10.1002/ajpa.23732>
- Santure, S.K., Harn, A.D., Esarey, D. (1990). *Archaeological Investigations at the Morton Village and Norris Farms 36 Cemetery*. Illinois State Museum, Springfield.
- Scheuer, L., & Black, S. (2004). *The juvenile skeleton*. Elsevier.
- Schlager, S. (2017). Morpho and Rvcg–Shape Analysis in R: R-Packages for geometric morphometrics, shape analysis and surface manipulations. In *Statistical shape and deformation analysis* (pp. 217-256). Academic Press.
- Sims, D. T., Burden, A., Payton, C., Onambélé-Pearson, G. L., & Morse, C. I. (2019). A quantitative description of self-selected walking in adults with Achondroplasia using the gait profile score. *Gait and Posture*, 68, 150–154. <https://doi.org/10.1016/j.gaitpost.2018.11.019>
- Sims, D. T., Burden, A., Payton, C., Onambélé-Pearson, G. L., & Morse, C. I. (2020). A spatio-temporal and kinematic description of self-selected walking in adults with Achondroplasia. *Gait and Posture*, 80, 391–396. <https://doi.org/10.1016/j.gaitpost.2020.06.030>
- Slice, D. E. (2005). *Modern morphometrics in physical anthropology*. Springer Science & Business Media.
- Slon, V., Nagar, Y., Kuperman, T., & HersHKovitz, I. (2013). A case of dwarfism from the byzantine city rehovot-in-the-negev, Israel. *International Journal of Osteoarchaeology*, 23(5), 573–589. <https://doi.org/10.1002/oa.1285>
- Sorrentino, R., Stephens, N.B., Marchi, D., DeMars, L. J. D., Figus, C., Bortolini, E., Badino, F., Saers, J. P. P., Bettuzzi, M., Boschini, F., Capecchi, G., Feletti, F., Guarnieri, T., May, H., Morigi, M.P., Parr, W., Ricci, S., Ronchitelli, A., Stock, J. T., Carlson, K. J., Ryan, T. M., Belcastro, M. G., Benazzi, S. (2021). Unique foot posture in Neanderthals reflects their body mass and high mechanical stress. *Journal of Human Evolution*, 161, 103093. <https://doi.org/10.1016/j.jhevol.2021.103093>
- Sorrentino, R., Stephens, N. B., Carlson, K. J., Figus, C., Fiorenza, L., Frost, S., Harcourt-Smith, W., Parr, W., Saers, J., Turley, K., Wroe, S., Belcastro, M.G., Ryan, T.M. Benazzi, S. (2020a). The influence of mobility strategy on the modern human talus. *American Journal of Physical Anthropology*, 171(3), 456–469. <https://doi.org/10.1002/ajpa.23976>
- Sorrentino, R., Belcastro, M. G., Figus, C., Stephens, N. B., Turley, K., Harcourt-Smith, W., Ryan, T.M., & Benazzi, S. (2020b). Exploring sexual dimorphism of the modern human talus through geometric morphometric methods. *PloS one*, 15(2), e0229255. <https://doi.org/10.1371/journal.pone.0229255>
- Sorrentino, R., Carlson, K. J., Bortolini, E., Minghetti, C., Feletti, F., Fiorenza, L., Frost, S. R.,

- Jashashvili, T., Parr, W., Shaw, C., Su, A., Turley, K., Wroe, S., Ryan, T., Belcastro, M.G., & Benazzi, S. (2020c). Morphometric analysis of the hominin talus: Evolutionary and functional implications. *Journal of Human Evolution*, 142, 102747. <https://doi.org/10.1016/j.jhevol.2020.102747>
- Sparacello, V. S., Marchi, D., & Shaw, C. N. (2014). The Importance of considering fibular robusticity when inferring the mobility patterns of past populations. In Carlson, K.J., Marchi, D. (Eds.), *Reconstructing mobility* (pp. 91–110). Springer, Boston, MA. <https://doi.org/10.1007/978-1-4899-7460-0>
- Stephens, N. B., Kivell, T. L., Pahr, D. H., Hublin, J. J., & Skinner, M. M. 2018. Trabecular bone patterning across the human hand. *Journal of Human Evolution*, 123, 1–23. <https://doi.org/10.1016/j.jhevol.2018.05.004>
- Tingran, G., Winchester, J., Stephens, N. B. (2020). Auto3dgm-matlab-gorgon: Auto3dgm with Transformation Matrices. Zenodo. Github.com/NBStephens/auto3dgm-matlab-gorgon. <https://doi.org/10.5281/zenodo.4006528>. Deposited 18 November 2020
- Traversari, M. (2017). *Ricostruzione del profilo bioculturale e biodemografico di una piccola comunita'montana del XVI-XVIII secolo attraverso i dati archeoantropologici e documentari: il caso degli inumati di Roccapelago (Modena)* (doctoral dissertation). Alma Mater Studiorum Università di Bologna (alma), Bologna. <https://doi.org/10.6092/unibo/amsdottorato/8205>
- Traversari, M., Da Via, S., Petrella, E., Feeney, R. N. M., & Benazzi, S. (2020). A case of dwarfism in 6th century Italy: Bioarchaeological assessment of a hereditary disorder. *International Journal of Paleopathology*, 30, 110–117. <https://doi.org/10.1016/j.ijpp.2020.03.003>
- Trinkaus, E. (2005). Anatomical evidence for the antiquity of human footwear use. *Journal of Archaeological Science*, 32, 1515–1526. <https://doi.org/10.1016/j.jas.2007.12.002>
- Turley, K., White, F.J., & Frost, S. R. (2015). Phenotypic plasticity: The impact of habitat and behavior (substrate use) on adult talo-crural appositional articular joint shape both between and within closely related hominoid species. *Human Evolution*, 30(1–2), 49–67. <https://doi.org/10.14673/HE201512002>
- Vazzana, A., Traversari, M., Frigerio, M., Buti, L., Dipino, N., Scalise, L. M., Motta, F., Rossi, A., Da Via, S., Gruppioni, G., Benazzi, S. (2017) Analisi Antropologica delle necropoli tardoantiche di Modena, In: *Mutina splendidissima. La città romana e la sua eredità*. De Luca Editori d'Arte srl, Roma, pp. 405 - 415.
- Vossen, J. A., Abbassi, M., Qian, Y., Hayes, C. W., Haar, P. J., Hoover, K. B. (2020). Correlation between the accessory anterolateral talar facet, bone marrow edema, and tarsal coalitions. *Skeletal Radiology*, 49(5), 699-705.
- Waters-Rist, A. L., & Hoogland, M. L. P. (2013). Osteological evidence of short-limbed dwarfism in a nineteenth century Dutch family: Achondroplasia or hypochondroplasia. *International Journal of Paleopathology*, 3(4), 243–256. <https://doi.org/10.1016/j.ijpp.2013.08.004>
- Wynne-Davies, R., Walsh, W. K., & Gormley, J. (1981). Achondroplasia and hypochondroplasia. Clinical variation and spinal stenosis. *Journal of Bone and Joint Surgery - Series B*, 63(4), 508–515. <https://doi.org/10.1302/0301-620x.63b4.7298674>



Fig. 1. The skeletal remains of T17.



Fig. 2. Left and right lower limbs of T17. Scale bar equals to 5 cm.

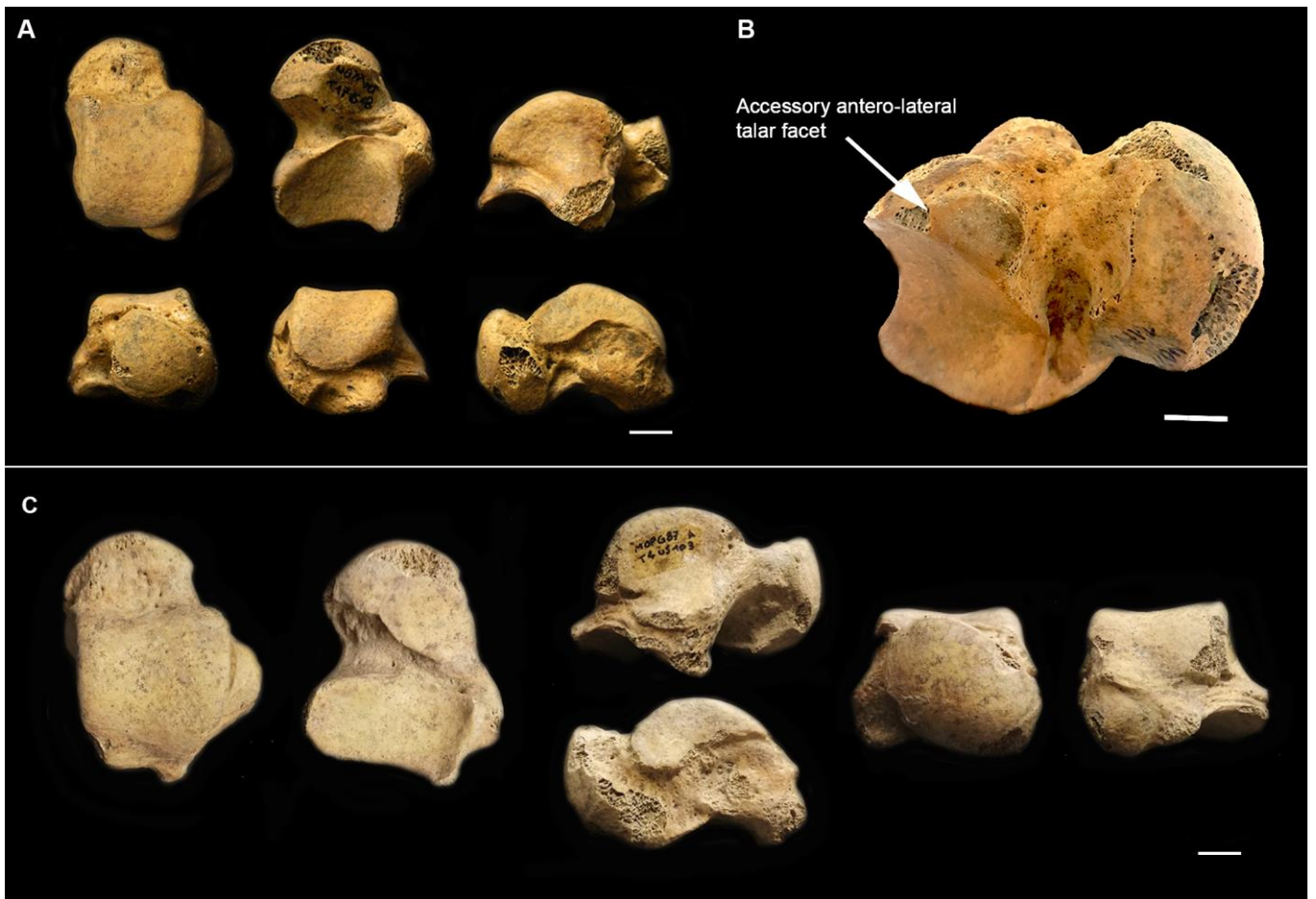


Fig. 3. The right talus of T17 shown in dorsal, plantar, and lateral views (A) in the top row (from left to right), and anterior, posterior, and medial views in the bottom row (from left to right). The accessory antero-lateral talar facet of the right talus of T17 (B). Comparison with a talus from the Modena group (C) shown in dorsal, plantar, and lateral (at the top), medial (at the bottom), anterior and posterior views (from left to right). Scale bar equals to 1 cm.

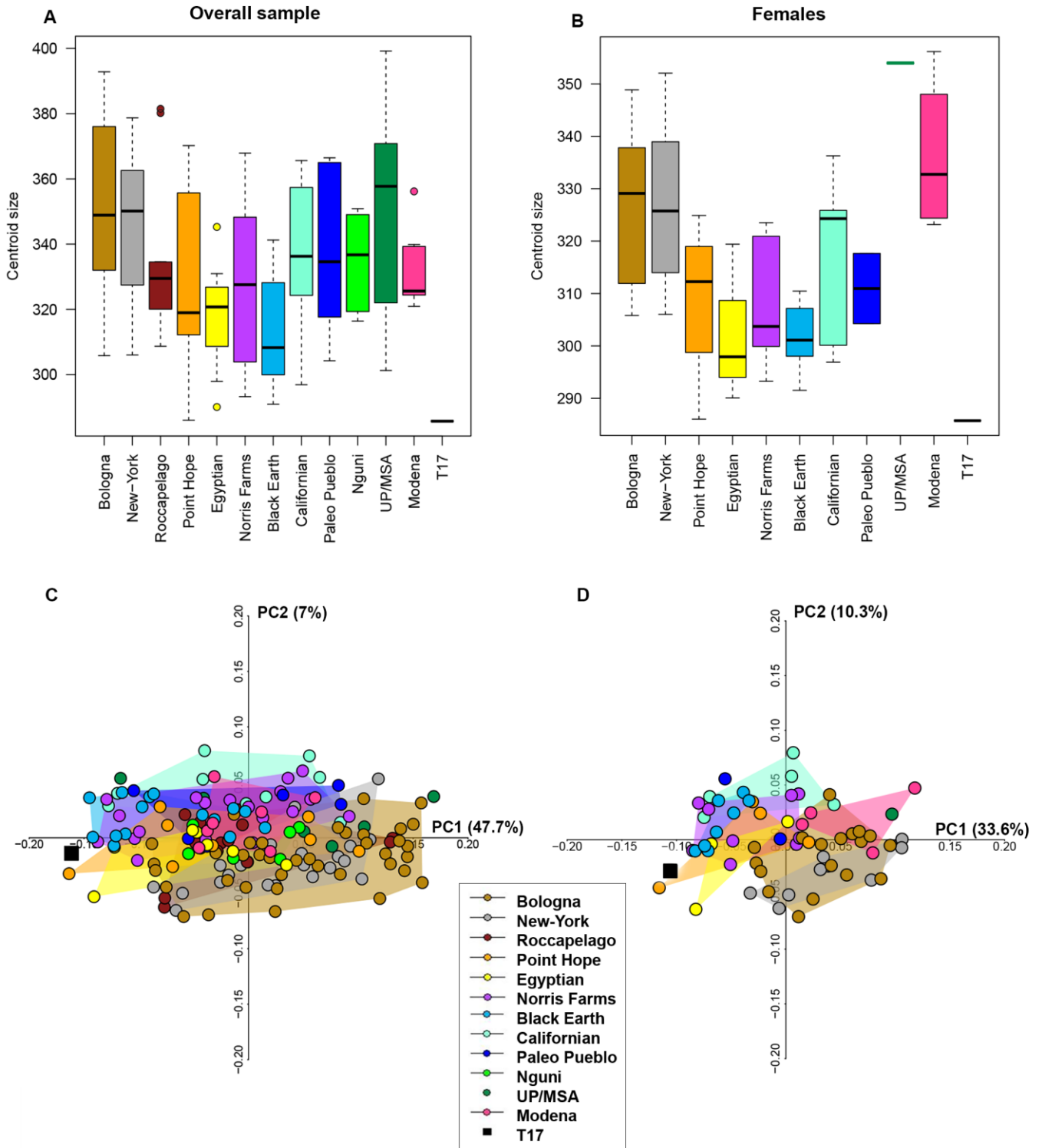


Fig. 4. Box-plots of talar centroid size distributions of the overall modern human groups and T17 (A), and the female only groups and T17 (B). Box components include the median (the horizontal bar), the upper and lower quartiles (limits of the boxes), and the extremes of each range (terminus of whiskers). Form space PCA plots of the overall modern human comparative sample (C) and only the female only groups (D), both including the hypochondroplastic T17.

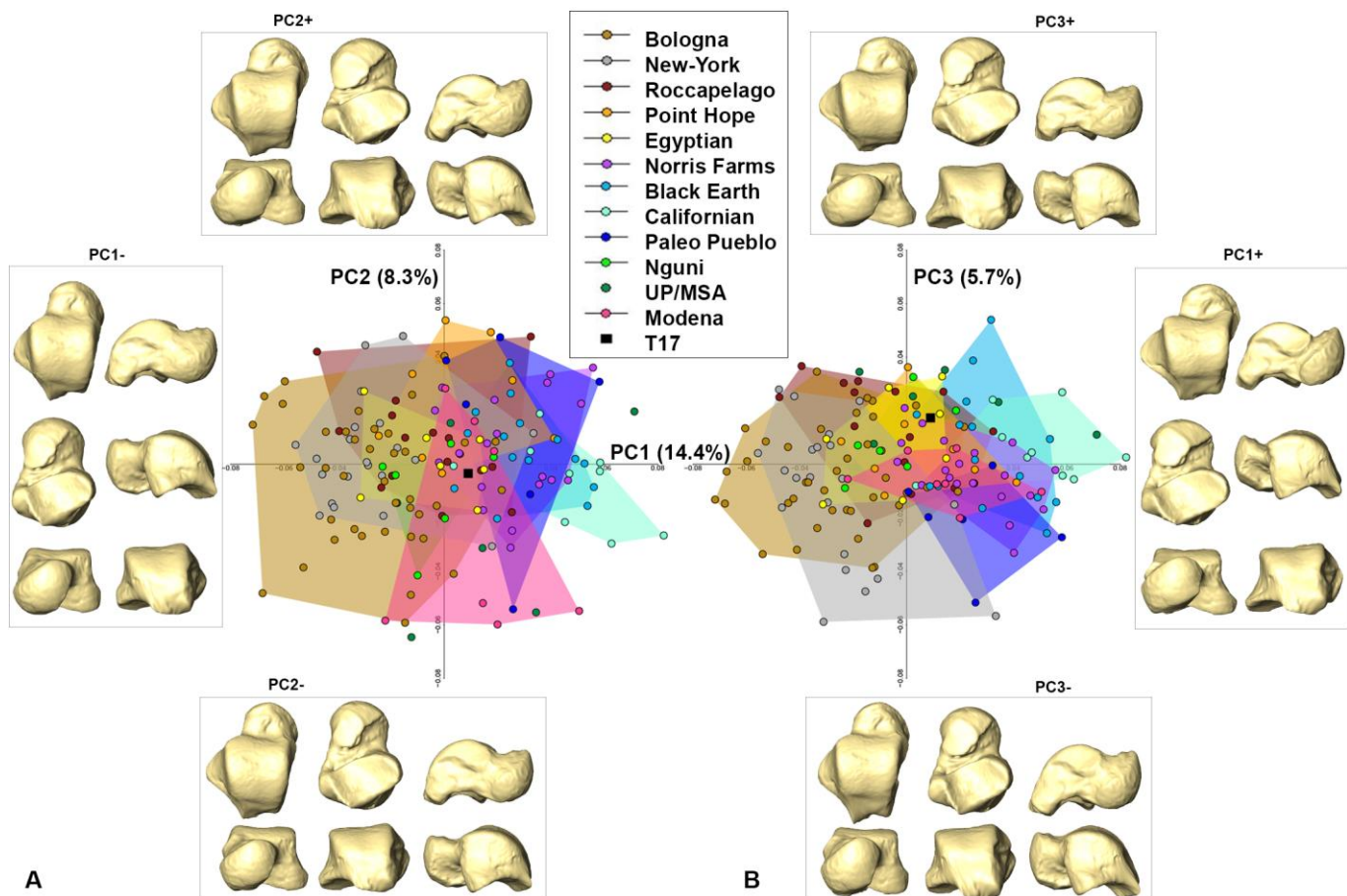


Fig. 5. Shape space PCA plots depicting PC1 vs PC2 (A) and PC1 vs. PC3 (B). The talus of T17 is projected in both PCA plots. Extreme shape changes along PC1 are shown in dorsal and medial in the first row (from left to right), inferior and lateral in the second row (from left to right), and anterior and posterior in the third row (from left to right). Extreme shape changes along PC2 and PC3 are shown in dorsal, plantar, and medial views in the top row (from left to right), and anterior, posterior, and lateral views in the bottom row (from left to right) within each box.

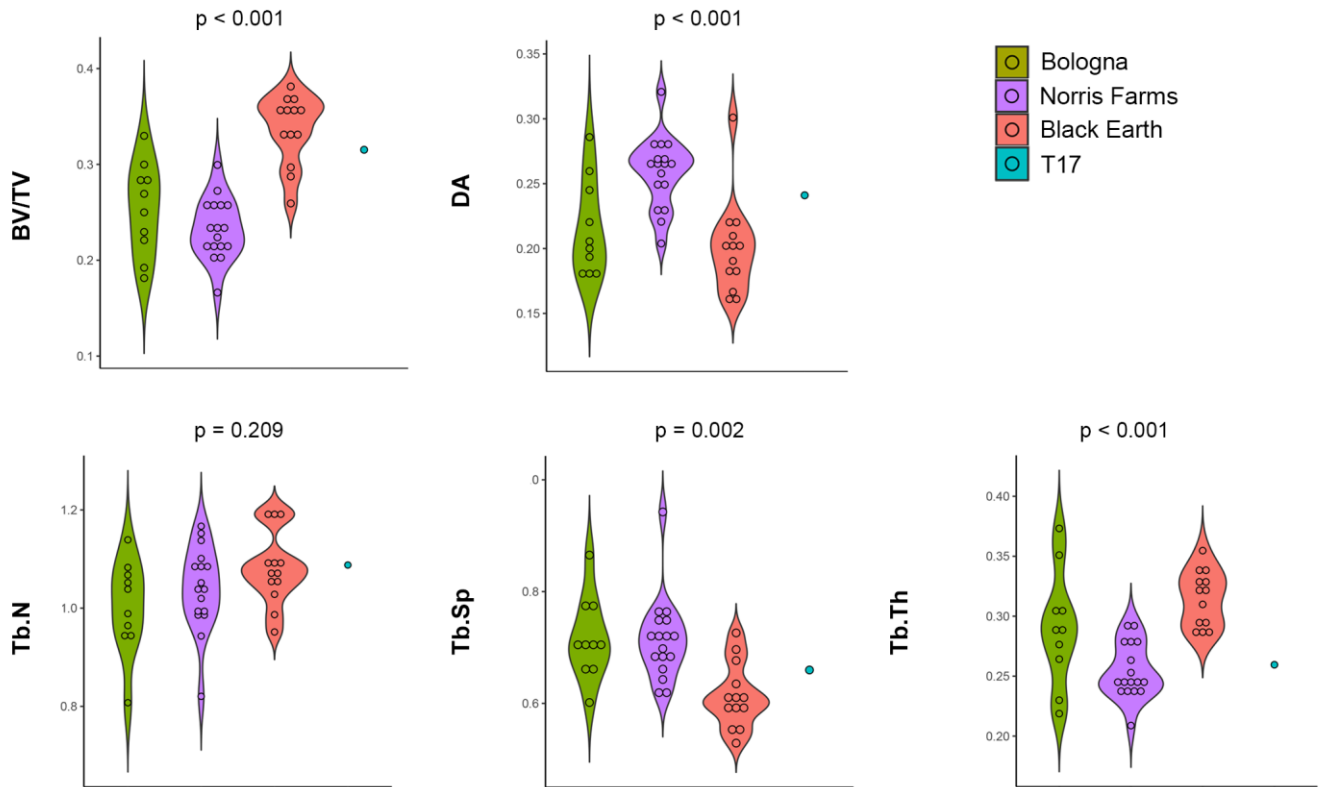


Fig. 6. Violin plots of bone volume fraction (BV/TV), degree of anisotropy (DA), trabecular spacing (Tb.Sp), trabecular thickness (Tb.Th), and trabecular number (Tb.N) by group. Violin components include each observation as a point and kernel bandwidth. The p-values for Kruskal-Wallis tests are reported above each plot, while Dunn test pairwise comparisons are reported in Table 5. Note that the T17 talus is excluded from these tests.

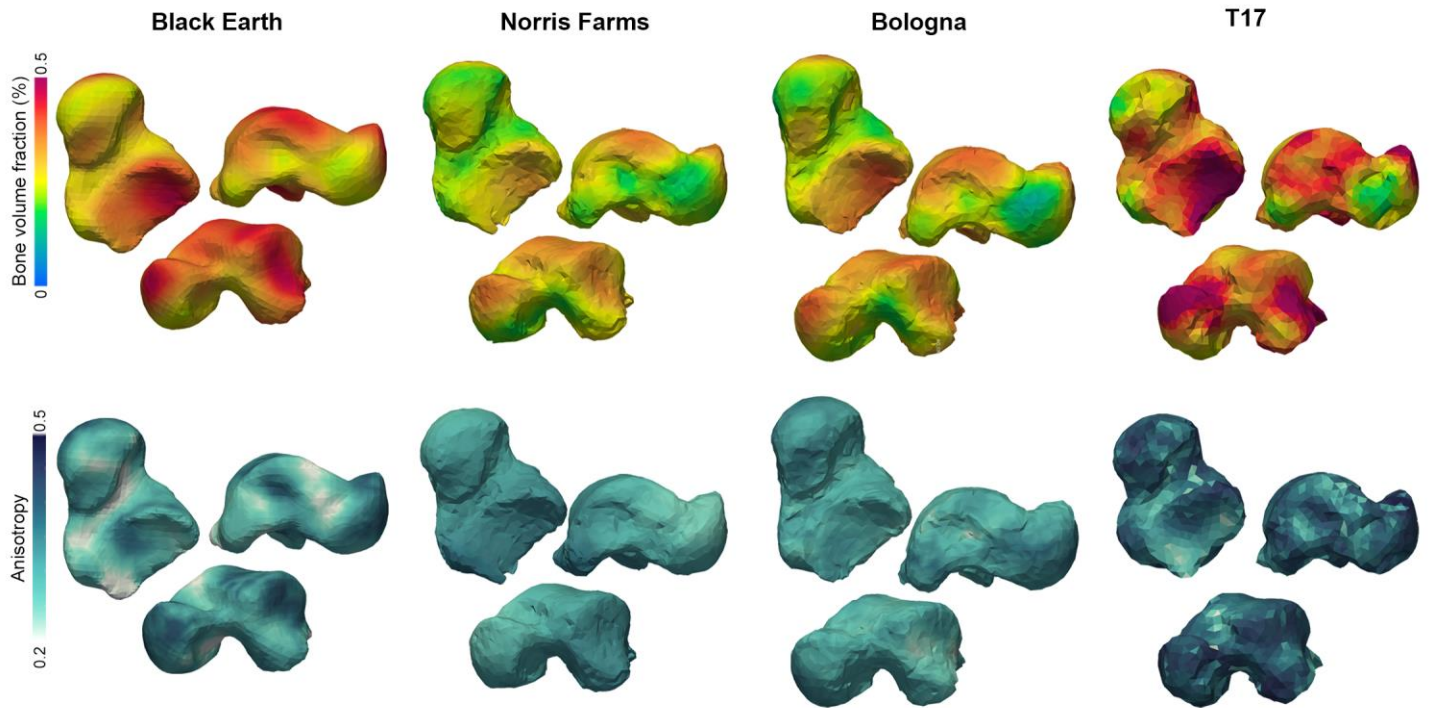


Fig. 7. Trabecular bone volume fraction (top row) and degree of anisotropy (bottom row) for the T17 talus and the average of Black Earth, Norris Farms and Bologna groups. Sets of tali are represented in plantar (top left), medial (top right) and antero-dorso-lateral (bottom) views, respectively. Scale at the top left represent variation of magnitude for bone volume fraction (warm colors indicate higher bone fraction), and scale at the bottom left represent degree of anisotropy (dark blue colors indicate higher degree of anisotropy).

Table 1. The sample used in the study.

Sample	N GM ¹	N trab ²	Chronological period	Geographical origin	Type of subsistence	Collection ³
UP/MSA ⁴	6	-	Upper Paleolithic / Middle Stone Age	Italy; Ethiopia	Hunters - gatherers	DBP/ NHMP
Black Earth	15	13	3000 B.C.	Illinois, USA	Hunters - gatherers	SIU
Californian	9	-	Shell Midden Cultures (~1500 d.C. - 500 A.D.)	California, USA	Hunters - gatherers	PAHM
Norris Farms	20	17	Late Prehistoric North America (1300 a.C.)	Illinois, USA	Mixed agriculture and foraging	ISM
Point Hope	8	-	~1600 - 500 A.D.	Alaska, USA	Maritime subsistence	AMNH
Egyptian	7	-	~600 - 350 A.D.	Egypt	Maritime subsistence/ farmers	AMNH
Paleo Pueblo	6	-	~1000 A.D.	New Mexico, USA	Mountain dwellers	AMNH
Roccapelago	15	-	XVII/XVIII century	Italy	Mountain dwellers	SAPAB
Nguni	6	-	XX century	South Africa	Farmers	BiGeA
Bologna	39	10	XIX/XX century	Italy	Post-industrial	BiGeA
New York	21	-	XX century	New York, USA	Post-industrial	NMNH
Modena	7	-	Late Ancient Period (IV/VII century)	Modena, Italy	Farmers, crafts and commerce	SAPAB
T 17	1	1	Late Ancient Period (VI century)	Modena, Italy	Farmers, crafts and commerce	SAPAB

¹Number of individuals used for Geometric Morphometric analyses.

²Number of individuals used for trabecular analyses.

³DBP, Department of Biology, University of Pisa, Pisa; NHMP, The Natural History Museum, Department of Earth Sciences, London; SIU, Southern Illinois University, Carbondale; PAHM, P. A. Hearst Museum Collections, University of California, Berkeley; ISM, Illinois State Museum, Springfield; AMNH, American Museum of Natural History, New York; SAPAB, Soprintendenza Archeologia, Belle Arti e Paesaggio per la città metropolitana di Bologna e le province di Modena, Ferrara e Reggio Emilia; BiGeA, Department of Biological, Geological and Environmental Sciences, University of Bologna, Bologna; NMNH, National Museum of Natural History, Smithsonian, Washington.

⁴UP, Upper Paleolithic (Romito7, Romito 8, Romito 9, Veneri 2 and Villabruna); MSA, Middle Stone Age (Clark Howell Omo, Ethiopia).

Table 2. Mean and standard deviation (SD) of talar centroid sizes across modern human groups¹.

	Female			Male			Total		
	Mean	SD	N	Mean	SD	N	Mean	SD	N ²
BOL	326.2	13.6	18	372.8	15.1	21	351.3	27.5	39
EGYP	302.4	15.2	3	329.9	11.2	4	318.1	18.8	7
PH	308.8	16.4	4	348.6	24.8	4	328.7	28.8	8
NF	309.3	12.6	9	347.1	11.1	10	327.9	22.6	20
MO	336.6	15.2	4	328.4	9.2	3	332.8	12.7	7
CA	316.7	17.3	5	356.6	9.9	4	334.4	25.1	9
NY	327.9	16.6	9	358.0	14.5	12	345.1	21.4	21
PP	310.9	9.5	2	350.2	20.3	4	337.0	26.0	6
RO	-	-	-	-	-	-	332.5	21.4	15
UP/MSA	353.9	-	1	377.2	19.6	3	351.4	35.1	6
NG	-	-	-	334.8	15.2	6	334.8	15.2	6
BE	301.8	6.2	8	325.8	16.4	7	313.0	17.0	15
T17	285.7	-	1	-	-	-	285.7	-	1

¹UP/MSA, Upper Paleolithic and Middle Stone Age; BE, Black Earth; CA, Californian; NF, Norris Farms; PH, Point Hope; EG, Egyptian; PP, Paleo Pueblo; RO, Roccapelago; NG, Nguni; BO, Bologna; NY, New York; MO, Modena.

²The total number includes males, females, and individual with unknown sex.

Table 3. Permutation test of differences in talar morphology among modern human groups¹. Significant *p*-values (*p* < 0.05) are in bold.

	BE	BOL	EGYP	PH	NF	MO	CA	NY	PP	RO	UP/MSA
BOL	0.006										
EGYP	1	1									
PH	1	0.016	1								
NF	1	0.006	1	1							
MO	1	0.068	1	0.246	1						
CA	1	0.006	0.107	0.068	1	1					
NY	0.006	1	1	0.193	0.006	0.011	0.006				
PP	1	0.006	1	1	1	1	1	0.027			
RO	0.115	0.158	1	1	0.117	0.268	0.006	0.287	0.262		
UP/MSA	1	0.006	1	0.356	0.791	1	1	0.006	0.220	1	
NG	1	1	1	1	1	1	0.192	1	0.881	1	1

¹UP/MSA, Upper Paleolithic and Middle Stone Age; BE, Black Earth; CA, Californian; NF, Norris Farms; PH, Point Hope; EG, Egyptian; PP, Paleo Pueblo; RO, Roccapelago; NG, Nguni; BO, Bologna; NY, New York; MO, Modena.

Table 4. Whole talus mean and standard deviation for trabecular variables by group and age.

Group	BV/TV*		DA		Tb.N		Tb.Sp		Tb.Th	
	Mean	SD	Mean	SD	Mean	SD	Mean	SD	Mean	SD
Bologna	0.25	0.05	0.22	0.04	1.00	0.09	0.72	0.07	0.29	0.05
<35 years (n = 6)	0.28	0.04	0.20	0.03	0.97	0.11	0.72	0.09	0.31	0.04
>35 years (n = 4)	0.22	0.05	0.24	0.04	1.04	0.05	0.71	0.05	0.25	0.04
Norris Farms	0.23	0.03	0.26	0.03	1.04	0.09	0.71	0.07	0.25	0.02
<35 years (n = 14)	0.23	0.03	0.26	0.03	1.02	0.08	0.73	0.07	0.26	0.02
>35 years (n = 3)	0.24	0.02	0.24	0.02	1.12	0.04	0.65	0.03	0.24	0.00
Black Earth	0.34	0.04	0.20	0.04	1.08	0.07	0.61	0.06	0.31	0.02
<35 years (n = 9)	0.34	0.03	0.20	0.02	1.08	0.08	0.61	0.05	0.32	0.02
>35 years (n = 4)	0.33	0.05	0.21	0.06	0.87	0.08	0.62	0.07	0.31	0.02
T17	0.31	-	0.24	-	1.09	-	0.65	-	0.25	-

*Abbreviations: Bone volume fraction (BV/TV), degree of anisotropy (DA), trabecular number (Tb.N), trabecular spacing (Tb.Sp), trabecular thickness (Tb.Th), and standard deviation (SD).

Table 5. Dunn test pairwise comparisons of mean talar trabecular variables*.

Trabecular variables	Black Earth vs Norris Farms	Black Earth vs Bologna	Norris Farms vs Bologna
BV/TV	0.000	0.004	1
DA	0.000	1	0.016
Tb.N	0.705	0.112	0.816
Tb.Sp	0.001	0.006	1
Tb.Th	0.000	0.264	0.098

*Abbreviations: Bone volume fraction (BV/TV), degree of anisotropy (DA), trabecular number (Tb.N), trabecular spacing (Tb.Sp), trabecular thickness (Tb.Th). Significant (<0.05) p-values are in bold. A Bonferroni correction was run for multiple comparisons.

